Application of miniature fiber near infrared spectroscopy combined with chemometrics in predicting antioxidant activity of Sagittaria sagittifolia L. polysaccharides

Yuqin Feng
Jiangsu University
Yating Song
Jiangsu University
Yujie Qiu
Jiangsu University
Yuqing Duan (dyq101@ujs.edu.cn)
Jiangsu University
Haihui Zhang
Jiangsu University

Research Article

Keywords: polysaccharides, structural, ultrasonic extract, near infrared (NIR) spectroscopy, antioxidant activity

Posted Date: June 14th, 2022

DOI: https://doi.org/10.21203/rs.3.rs-1734131/v1

Abstract

Oxidative stress associated with the imbalance between the production of reactive oxygen species and the antioxidant capacity. It is important to select and employ a stable and rapid method to assay antioxidant activity. The aim of this study was to accurately predict the antioxidant activity of *S. sagittaria.* L polysaccharide (Sap) by miniature fiber near-infrared (NIR) spectroscopy combined with chemometrics. The optimal extraction conditions of Sap through multi-mode divergent ultrasound assisted method were as follows: ultrasonic power 180 W, liquid-to-material ratio 40 mL/g, extraction time 16 min and extraction temperature 77 ℃, and the yield of Sap was 21.24%. The molecular weight of Sap was approximately 120.5 kDa, and its monosaccharide components predominantly consisted of Rha (15.7%), Ara (12.9%), Man (1.6%), Glc (36.4%), and Gal (33.4%). The application of NIR spectroscopy for determination of DPPH, ABTS and hydroxyl radical scavenging rate of Sap solution (0.125-1 mg/mL), and the coefficient of prediction (R_p) were 0.9568, 0.9667 and 0.9652, respectively. In developing model, five spectra preprocessing methods and three different linear regressions tools (i.e., partial least squares (PLS), interval Partial least Squares (iPLS), synergy interval partial least square (Si-PLS)) were optimized to improve the predictability and stability of the models. The overall results revealed the miniature fiber NIR spectroscopy with PLS and Si-PLS regression tools showed better predictive property, which has the potential to measure antioxidant activity in Sap.

1. Introduction

Sagittaria sagittifolia L. (*S. sagittifolia* L.) is an important medicinal and edible functional food, containing multiple chemical compositions, especially its bulb is rich in total sugar (54.6%), protein (16.4%), fat (0.47%) and other nutrients beneficial to human health including, triterpenes, flavonoids and polysaccharides, etc [1]. Among them, *S. sagittifolia* L. polysaccharides (Sap) have attracted much attention due to their has great medicinal potential such as antioxidation [2], restraining hepatic injury [3], antibacterial [4] and anticarcinogen [5]. Due to these potential effects, *S. sagittaria* L. has been applied in functional foods, pharmaceuticals and cosmetics industries [6].

Oxidation is an important process associated with the reactive oxygen species (ROS) including ABTS, hydroxyl, DPPH and superoxide anion radicals in living organisms. When ROS has accumulated to certain degree in the living organisms and exceeds their antioxidant capacity, the question of oxidative stress disease result would arise naturally, some side effects may occur (cancer, aging and other diseases) [7]. Hence, it is of high importance in developing effective, safe and natural antioxidants for scavenging excessive ROS for keeping the organism healthy. Antioxidant capacity is an essential biological indicator of bioactive substances. At present, different types of colorimetric assays are employed to measure the antioxidant capacity of polysaccharides, such as 2,2-diphenyl-picrylhydrazyl (DPPH) radicals scavenging, 2, 2'-Azino-bis (3-ethylbenzothiazoline-6-sulphonic acid) diammonium salt (ABTS) radicals scavenging, hydroxyl free radicals scavenging [8–11]. The conventional wet-chemical analysis (test kit, antioxidant reagent) is well known and routinely used in different lab. However, each of these methods has disadvantages, including complex operation, expensive, and the molecular structures which may be altered or compromised by chemical reagent. In this regard, it is urgent to develop a high precision, economic, non-destructive and simple indirect determination technology for the antioxidant activity of polysaccharides, and this new technology will be bound to promote the development of food industry.

NIR spectroscopy combined with quantitative data and mathematical models has been proved to be an efficient, reliable and green method [12, 13]. The success of NIR spectroscopy derives from subtle differences in vibrational modes of chemical bond, functional groups on these samples [14]. Then, NIR spectroscopy converts absorb radiation into spectral data in the wavelength range of 800–2500 nm, and the content and structure of bioactive components can be predicted through combining the spectral data with mathematical models [14]. Currently, increasing evidence highlights that NIR spectroscopy has been successfully applied to enhance or replace antioxidant activity analysis. Chen, et al. applied NIR spectroscopy combined with different regression tools to determine the antioxidant activity of green tea [15]. Di, et al. tried to predict the antioxidant activity (DPPH, FARP, and ABTS) in bamboo leaf extract using NIR spectroscopy combined with

five regression methods [16]. In another study, Caramês et al. attempted to measure the bioactivity potential in freeze-dried Brazilian berry pulp using NIR spectroscopy and smartphone imaging [17]. All of the above studies showed that NIR spectroscopy may be a practicable in measurement of antioxidant activity. Our previous research found that *S. sagittaria* L. polysaccharides (Sap) possess potential antioxidant activity in the development of functional foods [18], and multi-mode divergent ultrasound treatment can effectively improve the composition, structure and antioxidant activity of Sap [5]. However, during the research process, the traditional analysis methods of antioxidant activity of polysaccharides brought us a lot of trouble because of their complex operation, low accuracy, high price and destruction of the components to be tested, which makes a better method more necessary. Inspired by the above studies, we intend to determine the antioxidant activity of Sap by NIR, which is believed to be a useful supplement in related fields.

In the present study, optimize the conditions for multi-mode divergent ultrasound assisted extraction Sap and its physicochemical structure was characterized through M*w*, monosaccharide composition and FT-IR, as well as the surface morphology through SEM and AFM. The antioxidant properties of Sap *in vitro* have been determined by use of ABTS, hydroxyl and DPPH radicals scavenging assays. Here, we present a novel approach that attempts to evaluate and predict the antioxidant (DPPH, ABTS, hydroxyl radicals scavenging) potential of Sap by miniature fiber optical NIR spectroscopy.

2. Materials And Methods

2.1. Materials

S. sagittifolia L. was collected from a local Farmer's market (Jiangsu province, China). Standard monosaccharides, sulfuric acid, sodium chloride, 1, 1-diphenyl-2-picrylhydrazyl (DPPH), 2, 2'-Azino-bis (3-ethylbenzothiazoline-6-sulphonic acid) diammonium salt (ABTS) were obtained from Sigma Chemical Co. (St. Louis, MO, USA). Other reagents of analytical grade were purchased from Sinopharm Chemical Reagent Co., Ltd. (Beijing, China).

2.2. Process design

2.2.1. Single factor experimental design

Sap was extracted by a divergent ultrasound device as previously described [5]. The effects of extraction temperature, ultrasonic time, material to liquid ration and ultrasonic power on the extraction process of Sap was studied. Among these factors, extraction temperature ranged from 70 to 90 ℃, ultrasonic time ranged from 5 to 25 min, ratio of liquid to raw material ranged from 10 to 50 mL /g, ultrasonic power ranged from 60 to 180 W, ultrasonic frequency was set at double frequency (28/40 kHz).

2.2.2. Box-Behnken experimental design

Based on single factor experiments, a Box-Behnken experimental design (BBD) including 17 experiments was used to determine the optimal values of each variable to obtain the max yield of Sap. The design of experimental was shown in Table 1S. The experimental data were applied for the model and processed according to the equation [19]:

$$Y = \beta_0 + \sum_{j=1}^{k} \beta_j X_j + \sum_{j=1}^{k} \beta_{jj} X_j^2 + \sum \sum_{i<j} \beta_{ij} X_j X_j$$

Where Y represents the estimated response, β_0, is intercept, β_j, β_{jj} and β_{ij} are the model coefficients of the linear, quadratic and interaction, respectively, while X_i and X_j are the coded independent variables.

2.2.3. Sample solution preparation

Based on the optimal preparation process, the Sap (1.25-10 mg) was allowed to fully disperse with distilled water (10 mL), prepare different concentrations of Sap solution (0.125-1 mg/mL). Then, Sap solutions was centrifuged at 8000 r /min for

15 min, and the supernatant was stored at 4 ℃ in a refrigerator and measured the antioxidant activity of sample.

2.3. Physicochemical characterization

2.3.1. Chemical analysis

Total carbohydrate was measured by phenol-sulfuric acid method [20]. A carbazole-sulfuric acid method assay was applied to quantify uronic acid content [21]. Coomassie brilliant blue assay was applied to determine protein content of polysaccharides [22]. The total phenolic contents of polysaccharides was measured by the Folin-Ciocalteau method [23].

2.3.2. Molecular weight determination

The molecular weight of Sap fraction were measured by high-performance size-exclusion chromatograph (HPSEC) instrument according to our previous method with some modifications [18]. The apparatus consists of a multiangle laser scattering (DH-II, Wyatt Technology, USA), differential refractive index detector (Agilent G1362A, USA) and two columns (shodex OHpak SB-805 and shodex OHpak SB-806). Determining of the weight average molecular weight (M*w*) distributions of Sap was performed with Astra software.

2.3.3 Monosaccharide composition

The monosaccharide composition of samples was analyzed by gas chromatography (GC) according Wang et al. with minor modification [24]. In Brief, the polysaccharide was hydrolyzed with 5 mL of 3 mol/L trifluoroacetic acid solution (TFA) at 110°C for 120 min. The resulting solutions was washed 3 to 4 times with 5 mL methanol until the TFA was completely removed. Whereafter, the reaction solution was blended with hydroxylamine hydrochloride (10.0 mg), pyridine (1.0 mL) at 90 ℃ for 30 min. The reaction was initiated by the addition of 1.0 mL of acetic anhydride lasted approximately 30 min. Derivatives were analyzed on an Agilent GC 7890A instrument (2010A, Shimadzu, Kyoto, Japan).

2.3.4. UV and FT-IR spectroscopy

Make up to 0.5 mg/mL of Sap solution with deionized water. The UV-Vis spectra of the samples were determined using an ultraviolet-visible spectrophotometer (C100, Varian, USA) in the 190–400 nm range. About 2 mg of the Sap was mixed with KBr (200 mg) was ground to a fine powder, and this mixture was determined by a Fourier transform infrared (FT-IR) (IS50, Nicolet, USA) at the vibration region of 4000 − 400 cm^{-1}.

2.3.5. Molecular morphology observation

The morphological identification of Sap was accomplished using the atomic force microscope (AFM) and scanning electronic microscope (SEM). The Sap solutions (10 ug/mL) were filtered through a 0.22 μm filter membrane. A 10 μL of Sap solution was dropped on the surface of fresh mica and dried naturally before determination. Then, topographical images of sample on mica were recorded by AFM equipment (Multimode 8 instrument, USA). Dried samples of the Sap were sputter-coated with gold film before observation, and the sample powder was conducted with a S3400N SEM equipment (Hitachi, Japan). Images were captured at a magnification of 200 and 1000 ×.

2.4 Prediction of antioxidant activity

2.4.1 Spectral acquisition

In this experiment, the spectra of all the Sap solutions were obtained by a NIRQUEST256-2.5 Vis-NIR spectrometer. The device consists of TP-300 immersed fiber optic probe and DH-2000-BAL UV-Vis-NIR light source (Ocean Optics., USA). Approximately 5 mL of the various concentrations of Sap solution was put in a sample cup (with dimensions of 1 cm of diameter and 10 cm of depth). The spectrum parameters were: resolution of 6.4 cm^{-1}, optical path length of 4 mm, recorded rang of 800–2500 nm, and scanning times of 32. The schematic diagram of miniature fiber NIR spectroscopy system for determination of antioxidant activity in Sap (Fig. S1.). The spectral data of Sap were divided into two subsets:

all 120 samples contained calibration and prediction set. Among them, 90 samples as calibration set to establish the calibrating models, 1 sample of every 4 samples were selected as an independent prediction set (30 samples) to evaluate the performance of the test models. In addition, the range of y-value of the calibration set should close to the prediction set (Table 1).

Table 1
Statistics of calibration and validation data set.

Parameter	Units	Subsets	S. N	Range (y-value)	Mean	S.D.
DPPH	%	Calibration set	90	44.356–76.154	56.684	8.445
		Prediction set	30	44.813–73.001	55.761	7.952
ABTS	%	Calibration set	90	23.177–95.547	66.003	22.12
		Prediction set	30	23.471–94.130	63.484	22.428
Hydroxyl radical	%	Calibration set	90	28.503–77.663	53.113	15.355
		Prediction set	30	29.744–74.565	51.138	14.887
[a] SD = standard deviation						
[b] S. N = sample number						

2.4.2 Reference measurement

The Sap was determined by the phenol-sulfuric acid method using glucose as a reference [25]. The yield of Sap was calculated as follows:

$$\text{Yield (\%)} = \frac{m}{M} \times 100$$

Where *m* is the weight of the Sap, and *M* is the weight of *S sagittifolia* L.

The DPPH radical scavenging capacity was performed based on a reported method [11]. Briefly, 1 mL of Sap solutions of different concentrations (mentioned in section 2.2.3) and 1 mL of DPPH ethanol solution (0.1 mM) were mixed for 30 min in the dark. The absorbance of the mixture was measured at 517 nm (A_1), ethanol was used as a blank control (A_0) and the absorbance of distill water instead of DPPH solution (A_2). The calculation is as follows:

$$\mathrm{DPPHradicalscavengingactivity}(\%) = 1 - \frac{\left(A_1 - A_2\right)}{A_0} \times 100$$

The ABTS radical scavenging capacity was determined as previously described [26]. 15 mL ABTS (7 mM) was reacted with 15 mL of $K_2S_2O_8$ (5 mM) solution for 12 h in the dark. After reaction, the ABTS solution was diluted to 15 times with distilled water. Then, 1 mL of Sap solution (mentioned in section 2.2.3) with different concentrations and equal volumes (1 mL) of $ABTS^+$ solution was mixed for 30 min in the dark. The absorbance of mixture was measured at 734 nm (A_1), Sap solution was used as blank control (A_0), ABTS solution was instead by distill water to determine the absorbance (A_2). The calculation is as follows:

$$\mathrm{ABTSradicalscavengingactivity}(\%) = 1 - \frac{\left(A_1 - A_2\right)}{A_0} \times 100$$

Hydroxyl radical scavenging was determined as described by Wu et al [27]. Briefly, 10 mL $FeSO_4$ solution (6 mM) was mixed with 10 mL salicylic acid ethanol solution (6 mM) and H_2O_2 (0.1%) at room temperature. After that, equal volumes (1 mL) of Sap solution with different concentrations (mentioned in section 2.2.3) was mixed at 37 °C for 30 min. The absorbance at 510 nm was measured using a microplate analyzer. The absorbance of the sample was replaced by distill water (A_0), the absorbance of sample (A_1) and the blank reagent (replace H_2O_2 with distilled water) (A_2). The calculation is as follows:

$$\mathrm{Hydroxylradicalscavengingactivity}(\%) = 1 - \frac{\left(A_1 - A_2\right)}{A_0} \times 100$$

2.4.3 Spectral preprocessing

Since NIR spectral may provide irrelevant information such as noise, overlapping bands, background, and light scattering so on, which impact directly the model performance. Therefore, the use of appropriate spectra preprocessing methods is very essential as it weaken or remove interference in the spectra. In this study, the original spectrum was performed using Unscrambler X 10.4 software to carry out the standard normal variate (SNV) to correct spectral focuses and scales individual [28]. Multiplicative scatter correction (MSC) was used for correct discrete differentiation effects in original spectrum [29]. The baseline correction is mainly contained two steps, offset correction and null-space projection with the offset-corrected spectra [30]. The Derivative (1st, 2nd Der) can effectively reduce spectral multiplicative and additive effects [31]. Then, on the basis of partial least squares (PLS) regression method, the performance of original spectrum and five preprocessing methods were compared, and then selected the optimal pretreatment method.

2.4.4 Multivariate calibration methods

PLS is an interactive multiple linear regression model has been widely used in the quantitative analysis [32]. In the current study, the dimension reduction of high-dimensional data by spatial projection. The orthogonal eigenvectors of the independent and dependent variables is obtained, and then the unary linear regression is constructed. It not only overcomes the collinearity problem, but also eliminates the influence of noise on regression, so that the number of variables contained in the model is the least. The interval partial least Squares (iPLS), based on the PLS algorithm in which the full-spectrum data of sample is subdivided in several equally spaced intervals, and use of the PLS algorithm to select one interval of the highest predictive correlation [33]. Thus, the effects of no relevant or interference information was eliminated, which improved the prediction effect. The Synergy interval partial least square (Si-PLS) are commonly used as efficient variable selection methods to the non-destructive quantitative analysis fields [34]. The Si-PLS model is characterized by fast calculation speed and high precision, which can divide full-spectrum data into multiple efficient spectral subintervals, and equidistant interval combination.

2.4.5 Evaluation of the performance of the models

In this study, the coefficient of determination in calibration (*RMSEC*, R_c) or prediction (*RMSECP*, R_p) to evaluate the performance of calibration model. A good model shows higher R_p and lower *RMSEP*. Root mean square errors are calculated by:

$$RMSE = \sqrt{\frac{\sum_{i=1}^{n}(y_p - \hat{y}_q)^2}{n}}$$

where n is the training sample, y_p are the referenced value and $\hat{y}_q$ are the predicted value by the calibration set (*RMSECV*) or by an independent validation test (*RMSEP*), respectively.

R is calculated as follows:

$$R = \sqrt{1 - \frac{(y_p - \hat{y}_q)^2}{(y_p - \bar{y}_q)^2}}$$

y_p and $\hat{y}_q$ denote the measured and predicted value of the sample set; $\bar{y}_q$ denotes the mean of the measured value in sample set.

2.5. Software

All NIR spectra data were preprocessed and multivariate analyzed using the Unscrambler X10.4 and MATLAB R2014a software (Mathworks, Natick, USA). The models' tools refer to the method of Chen [14].

3. Results And Discussions

3.1 Single factor analysis

To study the effect of the extraction temperature of 70, 75, 80, 85 and 90°C on the extraction yield of Sap when the extraction power (120 W), time (15 min) and liquid to material ratio (30:1). The result shows that the yield of Sap increased when temperature increased from 70 to 80 ℃, but then decreased (Fig. S2A). This may be because that the solubility of solute in solvent increases with the increase of temperature [35]. In addition, the viscosity of solvent decreased, which improved the diffusivity of solvent in the tissue [36]. With further increase in extraction temperature, the cavitation effect is gradually weakened, which led to the yield decreased. Therefore, the extraction temperature was selected 80 ℃.

Extraction was carried out at different extraction time (5, 10, 15, 20 and 25 min) when the extraction temperature, power, and material to liquid ratio was 80℃, 120 W, 1:30, respectively. The yield of Sap increased when extraction time increased from 5 to 15 min and then the yield decreased (Fig. S2B). These results can be explained that the increasing ultrasonic time led to solvent permeated into the dried raw materials, which promote the release and diffusion of Sap [37]. However, the ultrasound treatment for the prolonged may result in the destruction of Sap structure and decrease the extraction rate [38]. Therefore, the extraction time was selected 15 min as the central point of the RSM experiments.

To study the effect of the different liquid to material ratio (10, 20, 30, 40 and 50) on the extraction yield of Sap when temperature, time and power was set at 80 ℃, 15 min, 120 W, respectively. The yield of Sap increased when LMR increased from 10 to 40 mL/g and then decreased (Fig. S2C). The extraction rate of Sap increase, on the one hand, can be attributed to the increase of cavitation effect with the decrease of solvent concentration, resulting in the diffusion of polysaccharides show more quickly [39]. On the other hand, the concentration difference between the intracellular and extracellular of plant cells can also promote the diffusion of polysaccharides [2]. However, the excess solvents may cause the decrease in distribution of energy of the ultrasonic wave and has a negative effect on the yield of polysaccharides [2, 38]. Thus, the LMR was set as 40 mL/g.

The effects of extraction power on Sap yield were investigated when the experiments conditions were fixed at 80 ℃, 15 min, 40:1 and the extraction power was set at 60, 90, 120, 150 and 180 W. The result shows that the yield of Sap increased with the increase in ultrasonic power from 60 to 150 W and then decreased (Fig. S2D). This may be due to the bubble size increases with the increase in the ultrasonic power, resulting in the implosion also intensifies [40]. The cells are broken and can effectively improve the diffusivity and extraction yield. In addition to that the high ultrasound intensity may damage the structure of polysaccharides reducing the yield [41]. Therefore, the extraction power is selected 150 W.

3.2. Optimization of Sap extracting conditions

Based on the results of single factor experiments. The main independent variables (*A*: ultrasonic power, *B*: ultrasonic time, and *C*: ultrasonic temperature) on the yield of Sap was displayed in Table 1. The yields of Sap ranged from 13.99–21.09% in the 17 experiments, such relatively great difference in extraction yield could be because the surface damage degree of the sample is different with the change of ultrasonic condition, and the amount of polysaccharide from the particles to the solution is also changed [2]. Thus, the optimized ultrasonic extraction parameter are required to improve the yield of Sap. In this study, multiple regression analysis and a second-order polynomial equation, generated by Design-Expert 12.0 software, were used to explain the relationship among three factors and responses. The final simplified equation for Sap extraction yield Y_1 in terms of coded parameters is:

$$Y_1 = 20.06 + 1.59\,A + 0.65\,B - 1.38\,C + 0.12\,AB - 1.18\,AC + 0.35\,BC - 1.29\,A^2 - 1.99\,B^2 - 1.91\,C^2$$

Where Y_1, *A*, *B*, *C* is extraction yield, ultrasonic power (W), ultrasonic time (min), and ultrasonic temperature (℃), respectively.

The fitting degree of model plays an important role in statistics. The Variance (*ANOVA*) and correlation coefficients (For coefficients R^2 and adjusted R^2) were the main methods of expression. Y_1 is highly significant with a high *F* value (62.77) and low *p*-values ($p < 0.0001$), which proved that the regression model is significant (Table S2),. Moreover, the value of correlation coefficient R^2 (0.9878) and adjusted R^2_{Adj} (0.972) are almost 1, which can explain the model is a high degree of correlation. The affecting of parameters on extraction process: A > C > B ($p > 0.05$), which might be due to the large polysaccharide particles are decomposed into smaller particles led to improving the yield under the diffusion of strong splitting force [2]. In terms of the interactions, the synergistic (positive) effect between the ultrasonic power and temperature (*AC*) is the most prominent ($p < 0.01$), which can improve the polysaccharide yield. This may be because both factors (*AC*) possess the capacity of destructive. As the power and temperature increases, yielded higher overall driving force, which led to the effect of extraction time is more significant. This means that the mild extraction conditions (low level) may yield a positive effect. When the extraction conditions are harsher, the effect of *AC* as the dominant factor. On the other hand, the coefficient variation (C.V.: 2.24%) and Adeq. precision (23.79) demonstrated experimental values shows high reliability and precision. The linear coefficient (AB, BC: >0.05) were non-significant, and the term coefficients (A^2, B^2, C^2: <0.05) was found to be at a significant.

3.3. Response surface analysis

The 3D response surface and two-dimension contour plots are mainly applied to express the interactions between the dependent /independent variables when other variables are fixed at zero level. The trend of response values kept increasing with increase values of variables, and then decreased, that illustrates the response surface is steady (Fig. S3). The effect of interactions extraction time and power had no significant effect on extraction rates when the temperature was fixed. The yield of Sap gradually increased when time increased from 10 to 15.68 min and power increased from 120 to 177.11 W (Fig. S3A and S3B). The further increase of extraction time and power had the negative effect on Sap yield. The extraction temperature and power exhibited quadratic effects on the Sap yields (Fig. S3C and S3D). The extraction rate increased significantly with the increased of extraction temperature over the range of 75 ℃-76.86 ℃ and power increased over the range of 120-177.11 W. The extraction yield didn't increase when extraction time and power reached the maximum yield, which may be due to the polysaccharides degraded under the synergistic effect of higher temperature and higher ultrasonic power. The interactions of extraction temperature and time on the extraction yield of Sap. The extraction rate increased when the temperature and time increased in the ranges of 75 ℃ to 76.86 ℃ and 10 to 15.68 min, respectively (Fig. S3E and S3F). Then, the yield declined gradually when the extraction temperature and time exceeded the ranges. This could be because polysaccharides were decomposed under higher temperature and longer extraction time. Based on the prediction of mathematical model, the optimal conditions for obtaining the maximum yield of Sap (21.24%) were as follows: 177.11 W, 15.68 min, 40 mL/g, 76.86 ℃. To simplify the actual operation parameters, extraction power, temperature, time, and liquid to material ratio set at 180 W, 77 ℃, 16 min; 40 mL/g.

3.4. Physicochemical properties of Sap

After analysis, the total carbohydrate content of the Sap extracted from the *S sagittifolia* L. was 79.26 ± 0.39% as determined by the phenol-sulfuric acid colorimetric method (Table 2). Moreover, the polyphenolic composition has been shown to affect the antioxidant activity of active substance, we also investigated whether the polyphenolic composition of Sap affects their antioxidant capacity. But no phenolic content was detected in Sap. Protein content was determined to be 2.67 ± 0.06%, these findings are consistent with the UV weak absorption peak was recorded at 280 nm for protein (Fig .1A). Additionally, the uronic acid was also detected, the content of uronic acid in Sap 1.33 ± 0.24%. M*w* play an important role in biological activities of polysaccharides. The M*w* and the molecular weight distribution coefficients (Mw/Mn) of Sap was 120.5 kDa and 1.591 (Fig. 1B). Moreover, it was shown that when the polydispersity index of the samples are smaller than 2 could imply that samples is less likely to form large sized agglomerate in aqueous solution [18]. The monosaccharide composition of Sap was determined to be mainly composed of rhamnose, arabinose, mannose, glucose, galactose and the molar ratio was 15.7: 12.9: 1.6: 36.4: 33.4 in Sap (Fig. 1C, Table 2). The Sap has the characteristic absorption peaks of carbohydrates as determined by FT-IR (Fig. 1D). In detail, the signal at 3422 cm^{-1} (O-H stretching vibration) and 2933 cm^{-1} (C-H stretching vibration) represents the characteristic groups of polysaccharides [24]. In particular, the absorption at 1735 cm^{-1} and 1654 cm^{-1} is related to the uronic acid (C = O stretching vibrations) and proteins, respectively. The band at 1000–1200 cm^{-1} are attributed to the bond stretching vibrations of C-O-C and O-C-O bonds reflects the presence of pyranose [42]. The signal at 900 cm^{-1} and 836 cm^{-1} represents the feature of β-glycosidic linkages and α-type glycosidic linkages, respectively [43].

Table 2
Composition of *Sap*.

Total carbohydrate (%)	Total phenolic	Protein (%)	Uronic acid (%)	Mw (kDa)	Mn	Mw/Mn	Monosaccharide compositions (mol%)				
							Rha	Ara	Man	Glc	Gal
79.26 ± 0.39	N. D	2.67 ± 0.06	1.33 ± 0.24	120.5 (± 0.804%)	75.76 (± 0.317%)	1.591 (± 0.865%)	15.7	12.9	1.6	36.4	33.4

Note: Each value represents the mean ± standard deviation (n = 3). N.D.: Not detected or below the limit of quantification. (Rha:Rhamnose, Ara:Arabinose, Man:Mannose, Glc:Glucose, Gal:Galactose)

The morphology and chain conformation are a critical indicator of polysaccharides involved in a variety of biological activities. We made use of AFM to visualize Sap has a compact globular architecture and a vast number of uneven lumps structure (Fig. 2A). The characteristic structures of Sap were examined by SEM image of 200 and 1000-fold magnification and its displayed as non-uniform and broken microsphere fragment's structure (Fig. 2B). The action of ultrasonic cavitation may be destructive to the microstructure of samples to expose more active sites, which may enhance biological activity.

3.5. Analysis of spectral preprocessing

The DPPH, ABTS and hydroxyl radical scavenging rate increased with the increase of Sap concentration (Fig. S3). The free radical scavenging rate trends of Sap at varied concentrations was in agreement with the reported results [18]. It can be observed that the original spectra of Sap changed when different preprocessing were employed (Fig. 3, Table 3). The correlation coefficients of the models of DPPH antioxidant activities were significantly improved by using MSC preprocessing. The reason for this phenomenon is because the scattered light of different particle sizes was removed by linear fitting each individual and reference spectrum. Therefore, the optimum PLS model was achieved when 8 PLS factors

and MSC spectra preprocessing were included in this work for DPPH (R_p = 0.9568 and *RMSEP* = 2.319%). The prediction by PLS model based on original spectra was superior to that of spectral preprocessing with higher R_p of 0.9651, 0.9602 and lower *RMSEP* of 6.160% and 4.265% for ABTS and hydroxyl radical, respectively.

Table 3
The results of PLS model based on different spectral preprocessing methods.

Parameter	spectral type	Calibration set (n = 90)			Cross-validation		Prediction set (n = 30)	
		LVs	Rc	RMSEC	Rcv	RMSECV	Rp	RMSEP
	Original	7	0.9686	2.01	0.9392	2.902	0.9410	2.710
DPPH	SNV	8	0.9850	1.459	0.9085	3.573	0.9525	2.430
	MSC	**8**	**0.9853**	**1.442**	**0.9049**	**3.643**	**0.9568**	**2.319**
	Baseline	8	0.9697	2.062	0.9413	2.855	0.9386	2.756
	Derivative I	6	0.9775	1.779	0.9116	3.475	0.9060	3.535
	Derivative II	4	0.9317	3.068	0.8232	4.796	0.8678	4.067
	Original	**6**	**0.9689**	**5.497**	**0.9457**	**7.231**	**0.9651**	**6.160**
	SNV	6	0.9696	5.435	0.9349	7.901	0.9440	7.652
ABTS	MSC	5	0.9579	6.381	0.9217	8.649	0.9319	8.482
	Baseline	6	0.9635	5.946	0.9384	7.700	0.9604	6.413
	Derivative I	5	0.9799	4.431	0.9501	6.946	0.9509	7.225
	Derivative II	4	0.9519	6.81	0.8744	10.79	0.8832	11.29
	Original	**6**	**0.9679**	**3.891**	**0.9486**	**4.904**	**0.9602**	**4.265**
	SNV	6	0.9680	3.886	0.9336	5.559	0.9465	4.966
	MSC	6	0.9689	3.831	0.9252	5.908	0.9430	5.177
Hydroxyl radical	Baseline	6	0.9647	4.079	0.9418	5.217	0.9550	4.569
	Derivative I	5	0.9696	3.789	0.9292	5.722	0.9253	6.014
	Derivative II	4	0.9394	5.307	0.8392	8.431	0.8570	8.432

3.6. NIR calibration results

3.6.1 Analysis of DPPH

As shown in Table 5, the model for DPPH scavenging activity showed an R_c of 0.9853, *RMSECV* of 1.442%, R_p of 0.9568 and *RMSEP* of 2.319% in the MSC-PLS model. The iPLS based model for DPPH scavenging activity, with 20 intervals for the full spectrum. Then the model of each subinterval was established. The predictive MSC-iPLS model of DPPH, the model

built on the 19 subintervals of the whole spectral interval was the best, which corresponds to the spectral interval of 1358.34-1439.97 nm, with the highest value of R_p =0.81 and *RMSEP* = 4.82% in the prediction.

The results showed that Si-PLS model of DPPH scavenging activity showed that the optimal number of LVs selected from the 4 intervals from 15 (Table 4). The optimal PCs was 9, and combinations of intervals selected were [1, 5, 10, 13], which corresponding to 868.6-977.4, 1303.8-1412.6, 1847.8-2065.4 and 2174.2–2283.0 nm in the spectral regions (Fig. 4A), the Si-PLS model yielded R_c= 0.9459, *RMSEC* = 2.76%, R_p= 0.9455 and *RMSEP* = 2.70%. The spectra regions are features of various unique constituents, mainly related to the combination of some functional group and overtones and vibrational modes such as -CH, -NH, -SH and -OH groups [44, 45]. We observed that the spectra regions 868.6-977.4 nm commonly associated to third C-H overtone of polysaccharides. At 1303.8-1412.6 nm, speculate that the variation of is related to the O-H first overtone. At 1847.8-2065.4 nm is due to the O-H stretching vibration and at 2174.2–2283.0 nm are derived from the C-H stretching vibration and CH_2 deformation. Compared with Si-PLS model of full spectra, MSC-PLS model showed good prediction effect. Figure 4D is the scatter plots that show DPPH estimated by MSC-PLS model in the prediction sets.

Table 4
Spectral subinterval of Si-PLS calibration model.

Parameters	Number of subintervals	PCs	Selected subintervals	R_C	RMSEC	R_P	RMSEP
DPPH	**15**	**9**	**[1, 5, 10, 13]**	**0.9459**	**2.76**	**0.9455**	**2.70**
	16	11	[5, 10, 11, 16]	0.9321	3.08	0.8837	4.06
	17	7	[1, 8, 11, 16]	0.9378	2.94	0.9361	2.95
	18	9	[6, 12, 15, 16]	0.931	3.10	0.8855	3.81
	19	10	[2, 5, 6, 12]	0.9347	3.01	0.8842	3.8
	20	9	[7, 13, 16, 17]	0.9375	2.95	0.9132	3.31
	21	9	[7, 13, 14, 18]	0.9246	3.24	0.9197	3.22
	22	10	[6, 7, 14, 18]	0.945	2.78	0.8928	3.84
	23	12	[7, 15, 16, 23]	0.9462	2.75	0.8389	5.54
	24	9	[8, 15, 16, 20]	0.9346	3.01	0.9306	3.17
	25	9	[8, 16, 17, 21]	0.9388	3.02	0.9259	3.21
	26	7	[1, 13, 16, 24]	0.9404	2.72	0.9360	2.97
	27	10	[8, 17, 18, 22]	0.9357	3.01	0.9249	3.22
	28	9	[9, 18, 19, 23]	0.9354	3.00	0.9163	3.38
	29	6	[1, 10, 14, 17]	0.9248	3.21	0.9251	3.03
	30	8	[9, 18, 19, 25]	0.9345	3.01	0.9226	3.07
ABTS	15	12	[2, 6, 10, 14]	0.9771	4.73	0.9214	9.06
	16	10	[1, 6, 11, 16]	0.9717	5.25	0.9617	7.57
	17	10	[2, 7, 11, 17]	0.9716	5.27	0.9542	7.46
	18	9	[2, 7, 12, 17]	0.9753	4.92	0.9351	8.12
	19	8	[2, 7, 9, 12]	0.9727	5.16	0.9607	6.4
	20	12	[2, 8, 17, 20]	0.9702	5.42	0.9514	7.02
	21	9	[2, 8, 9, 21]	0.971	5.32	0.9534	7.3
	22	9	[2,8, 9, 22]	0.9704	5.37	0.9507	7.45
	23	6	[2, 9, 12, 15]	0.9682	5.56	0.9457	7.58
	24	7	[2, 7, 9, 15]	0.9704	5.37	0.9408	8.09
	25	**9**	**[1, 12, 17, 24]**	**0.9693**	**5.47**	**0.9667**	**6.75**
	26	11	[3, 10. 17. 24]	0.9664	5.72	0.9016	10.6
	27	10	[3, 10, 12, 17]	0.9725	5.19	0.9352	8.31
	28	9	[2, 18, 19, 27]	0.967	5.66	0.9416	9.24
	29	10	[3, 11, 19, 27]	0.9669	5.68	0.9291	8.89

Parameters	Number of subintervals	PCs	Selected subintervals	R_C	RMSEC	R_P	RMSEP
	30	9	[3, 11, 13, 19]	0.9706	5.41	0.9316	8.6
Hydroxyl radical	15	10	[1, 7, 10, 15]	0.9644	4.11	0.9542	4.67
	16	9	[1, 8, 11, 15]	0.9507	4.83	0.9614	4.29
	17	9	[1, 8, 11, 17]	0.9693	3.81	0.9617	4.23
	18	8	[2, 5, 7, 9]	0.969	3.83	0.958	4.37
	19	9	[1, 9, 12, 19]	0.9696	3.79	0.9437	5.15
	20	8	[2, 8, 9, 17]	0.9691	3.82	0.9532	4.7
	21	8	[2, 6, 8, 10]	0.9702	3.75	0.9526	4.65
	22	11	[2, 6, 13, 19]	0.9681	3.89	0.9043	7.21
	23	**9**	**[2, 9, 10, 16]**	**0.9688**	**3.84**	**0.9652**	**4.22**
	24	7	[2, 7, 9, 12]	0.9709	3.71	0.955	4.55
	25	10	[2, 6, 11, 17]	0.9669	3.98	0.9537	4.93
	26	8	[2, 6, 17, 18]	0.9655	4.04	0.9426	6.13
	27	8	[2, 10, 11, 18]	0.9705	3.74	0.9568	4.84
	28	9	[2, 3, 12, 19]	0.9714	0.368	0.9651	4.91
	29	7	[2, 8, 11, 14]	0.9646	4.09	0.9582	4.46
	30	8	[2, 3, 13, 20]	0.9668	3.96	0.9532	5.01

Table 5
Comparison of different algorithms.

Parameter	Spectral type	LVs	Rc	RMSEC	Rp	RMSEP
DPPH	**MSC-PLS**	**8**	**0.9853**	**1.442**	**0.9568**	**2.319**
	MSC-iPLS	5	0.8376	4.61	0.8100	4.82
	MSC-Si-PLS	9	0.9459	2.76	0.9455	2.70
ABTS	PLS	6	0.9689	5.497	0.9651	6.160
	iPLS	6	0.8836	10.40	0.8747	12.00
	Si-PLS	**9**	**0.9693**	**5.47**	**0.9667**	**6.75**
Hydroxyl radical	PLS	6	0.9679	3.891	0.9602	4.265
	iPLS	5	0.8737	7.53	0.8712	7.59
	Si-PLS	**9**	**0.9688**	**3.84**	**0.9652**	**4.22**

3.6.2 Analysis of ABTS

As for ABTS scavenging activity, PLS model yielded R_c= 0.9689, *RMSECV* = 5.497% and R_p= 0.9651 and *RMSEP* = 6.16%. In iPLS model, the optimal model was built on the 19 subintervals of the full spectral interval, which corresponds to the

spectral interval of 1848.08-1929.70 nm, with R_c= 0.8836, *RMSECV* = 10.40% and R_p= 0.8747, *RMSEP* = 12% (Table 5). As shown in Table 4, the optimal spectral intervals selected by Si-PLS model for the prediction of ABTS. The optimal parameter of Si-PLS model was a combination of 4 from 25 intervals, the optimal LVs was 9, and combination of intervals selected were [1, 12, 17, 24], corresponding to 868.6-933.9, 1586.9-1652.2, 1913.4-1978.7 and 2370.5-2435.8 nm (Fig. 4B). The spectra regions at 868.6-933.9 nm are connected with the third C-H overtone. 1586.9-1652.2 nm is due to the first C-H overtone. The spectra regions around 1913.4-1978.7 nm were assigned to O-H stretching vibration, and that at 2370.5-2435.8 nm were assigned to C-H stretching vibration and CH_2 deformation. Figure 4E was the scatter plot showing ABTS estimated by Si-PLS model in the prediction sets. The highest R_p= 0.9667 and lowest *RMSEP* = 6.75%.

3.6.3 Analysis of Hydroxyl radical

As for the hydroxyl radical inhibition activity, the PLS model yielded R_c= 0.9679, *RMSECV* = 3.891% and R_p= 0.9602, *RMSEP* = 4.265%. In the iPLS model, the best model was built on 19 subintervals of the whole spectral interval, which corresponds to the spectral interval of 1358.34-1439.97 nm, with R_c= 0.8737, *RMSECV* = 7.53% and R_p= 0. 8712, *RMSEP* = 7.59% (Table 5). The optimal parameter of Si-PLS model was a combination of 4 intervals from 23 interval, the optimal LVs was 9, and the combinations of intervals selected were [2, 9, 10, 16], corresponding to 939.5-1010.4 nm, 1435.8-1506.7 nm, 1506.7-1577.6 nm and 1932.1–2003.0 nm (Fig. 4C), respectively. The spectra regions 939.5-1010.4 nm is mainly attributed to the second O-H overtone. 1435.8-1506.7 nm and 1506.7-1577.6 nm is due to the CH_3, CH_2, CH of polysaccharides. The spectra regions around 1932.1–2003.0 nm contributed from O-H stretching vibration. The scatter plot showing hydroxyl radical estimated by Si-PLS model in the prediction sets (Fig. 4F). Here, the R_p= 0.9652 and *RMSEP* = 4.22%. Compared with PLS and iPLS method, the Si-PLS models of values of R_p and R_c are higher, and *RMSECV* and *RMSEP* are lower.

4. Discussion

Three models showed good performance by using NIR spectrum acquisition and stoichiometric calculation, and the antioxidant activity of Sap is quickly detected in predictive set. The prediction performance of the three models varies in different degrees, and the reasons are as follows:

The PLS model of DPPH was better than that of iPLS and Si-PLS, which may be due to the effective spectral range of the main factors affecting DPPH was wide, and most useful information has not been selected. On the other hand, it may be because the correlation coefficient between the correction and prediction set of the full spectrum modeling is in the middle, no data will be lost when the full spectrum is used for modeling.

However, this full spectrum modeling method will introduce a lot of spectral information (information about impurities such as starch) that is independent of ABTS and hydroxyl radical scavenging rate. These irrelevant parameters and redundant variables could increase the computation burden, while lower the accuracy of modeling effect of PLS and reduce the prediction performance. In addition, there is also a high degree of collinearity among the full spectrum variables, and the intervention of these redundant information is bound to reduce the stability of the model to some extent. For ABTS and hydroxyl radical, compared with PLS and iPLS model, Si-PLS model cannot only eliminate a lot of useless spectral information, but also extract and use as much useful information as possible to establish the best prediction model by combining four relevant subintervals.

Compared with PLS and Si-PLS, iPLS model was the least effective. The main reason is that iPLS only used the data on one subinterval in modeling, and a large amount of data is deleted, and many characteristic data are not used. In addition, the parameters reflected by the spectral information in the extraction process collected by NIR mainly come from the frequency doubling and absorption of stretching vibration of different groups in Sap, and any single interval cannot completely reflect the spectral information. The iPLS model only selects a subinterval of the full spectrum to establish the

correction model, which will lose a lot of useful information. Ultimately, led to poor performance of both the correction set model and the prediction set model.

5. Conclusions

The study investigated an effective and feasible of the miniature fiber NIR spectra for the prediction of antioxidant activity of Sap. The result showed that the MSC-PLS model present excellent performance for DPPH. Si-PLS model is the most potential predictive model for ABTS and hydroxyl. It means that the NIR spectra is an applicable and good potential for rapid evaluation method of antioxidant activities.

In general, the content of polysaccharides extracted from raw materials is low and contains other active components and impurities, which may contribute less to the anti-oxidation effect, making it the difficult to monitor the antioxidation activity of polysaccharides online. Therefore, the obtained polysaccharides must be increased the concentration through alcohol precipitation, deproteinization, concentration and other processes. The off-line detection can provide guidance and reference for online monitoring of antioxidant activity of polysaccharides, and provide a new idea for online monitoring of biological activity in the future.

Declarations

Acknowledgement

This work is funded by the Postgraduate Research & Practice Innovation Program of Jiangsu Province, China **(KYCX21_3397)**; National Natural Science Foundation of China **(32072354)**; The Key R & D Program of Ningxia Hui Autonomous Region **(2022BBF03016)**; National Key Research and Development Program of China **(2016YFD0400303)**; Priority Academic Program Development of Jiangsu Higher Education Institutions **(PAPD)**.

Authors' Contributions Yuqin Feng: Funding acquisition, Project administration, Writing Original draft preparation. Yating Song: Validation. Yujie Qiu: Methodology. Yuqing Duan: Funding acquisition, Supervision, Writing-Review & Editing. Haihui Zhang, Investigation.

Conflict of Interest The authors declare that they have no known competing financial interests or personal relationships that could have appeared to influence the work reported in this paper.

References

1. J. Zhang, C. Wen, Y. Duan, H. Zhang, H. Ma, Int. J. Biol. Macromol. **134**(1), 172–179 (2019)
2. J. Gu, H. Zhang, J. Zhang et al., Carbohydr Polym. **246**, 116595 (2020a)
3. J. Wang, W. Luo, B. Li, Y. Liao, J. Ethnopharmacol. **227**(5), 237–245 (2018)
4. X. Liu, Q. Pan, Y. Shi, I. Williams, H. Sung, Z. Min, J. Nat. Prod. **69**(2), 255–260 (2006)
5. Y. Feng, I. Juliet, Y. Duan, H. Zhang, H. Ma, Food Bioscience **42**, 101145 (2021)
6. W. Ahmed, W. Ali, A. Gani, M. Ahmad, W. Ahmad, Food Bioscience **11**(1), 23–32 (2015)
7. C. Giorgi, S. Marchi, M. Simoes et al., Int. Rev. Cell. Mol. Biol. **340**, 209–344 (2018)
8. O. Yarley, A. Kojo, C. Zhou, H. Kwadwo, O. Richard, Int. J. Biol. Macromol. **183**(31), 2262–2271 (2021)
9. M. Ahmad, Carbohydr. Polym. Technol. Appl. **2**, 100045 (2021)
10. S. Milardovi, D. Ivekovi, B. Grabari, Bioelectrochemistry **68**(2), 175–180 (2006)
11. N. Khalaf, A. Shakya, A. Othman, Z. Agbar, H. Farah, Turkish J. Biology **32**(1), 51 (2008)
12. M. Andrew, P. Martinsen, C. Clark, R. Jordan, Postharvest Biol. Technol. **37**(2), 142–151 (2005)

13. H. Schulz, U. Engelhardt, A. Wegent, H. Drews, S. Lapczynski, J. Agric. Food Chem. **47**(12), 5064–5067 (1999)
14. Q. Chen, J. Zhao, M. Liu, J. Cai, J. Liu, J. Pharm. Biomedical Anal. **46**(3), 568–573 (2008)
15. Q. Chen, Z. Guo, J. Zhao, O. Qin, J. Pharm. Biomedical Anal. **60**(23), 92–97 (2012)
16. D. Wu, J. Chen, B. Lu, L. Xiong, Y. He, Y. Zhang, Food Chem. **135**(4), 2147–2156 (2012)
17. E. Caramês, M. Baqueta, D. Conceição, J. Pallone, Food Res. Int. **140**, 109792 (2021)
18. J. Gu, J. Zhang, Y. Duan, H. Ma, H. Zhang, Carbohydr. Polym. **235**(1), 115939 (2020b)
19. G. Box, D. Behnken, Technometrics **2**(4), 455–475 (2012)
20. A.-P.T. Miafo, B.B. Koubala, G. Kansci, G. Muralikrishna, J. Cereal Sci. **87**, 124–131 (2019)
21. T. BitterH, M. Muir, Anal. Biochem. **4**(4), 330–334 (1962)
22. C.Y. Liau, C.S. Lin, J. Biosci. Bioeng. **106**(1), 111–113 (2008)
23. E. Zambrzycka, E. Nalewajko, M. Zaremba, A. Bajguz, B. Godlewska, Molecules 25 (15) (2020)
24. K. Wang, J. Guo, J. Cheng et al., Int. J. Biol. Macromol. **191**, 1038–1045 (2021)
25. M. Dubois, K. Gilles, J. Hamilton, P. Rebers, F. Smith, Anal. Chem. **28**(3), 350–356 (1956)
26. R. Re, N. Pellegrini, A. Proteggente, Free Radic. Biol. Med. **26**(9–10), 1231–1237 (1999)
27. W. Wu, Y. Zhu, Z. Li, R. Yang, Y. Zhou, Carbohydr. Polym. **87**(2), 1348–1353 (2012)
28. B. Lu, X. Wang, N. Liu, C. Hu, X. Tang, Infrared Phys. Technol. **111**, 103482 (2020)
29. M. Zhu, Y. Long, Y. Chen et al., J. Food Compos. Anal. **102**, 104055 (2021)
30. H. Shinzawa, J. Mizukado, J. Mol. Struct. **1069**(1), 171–175 (2020)
31. S. Jun, Z. Xin, X. Wu, J. Shen, Spectrochim. Acta Part A Mol. Biomol. Spectrosc. **212**(5), 215–221 (2019)
32. G. Rossi, V. Lozano, LWT **126**, 109290 (2020)
33. R. Anisur, K. Naoshi, O. Yuichi, S. Tetsuhito, K. Katsuhiro, Biosyst. Eng. **141**, 12–18 (2016)
34. Y. Yang, L. Wang, Y. Wu, Y. Chen, Spectrochim. Acta Part A Mol. Biomol. Spectrosc. **182**(5), 73–80 (2017)
35. K. Kumar, S. Srivastav, V. Sharanagat, Ultrason. Sonochem. **70**, 105325 (2021)
36. C. Jiang, X. Li, Y. Jiao, D. Jiang, Q. Zhang, Carbohydr. Polym. **110**(22), 10–17 (2014)
37. C. Zhu, X. Zhai, L. Li, X. Wu, B. Li, Food Chem. **177**(15), 139–146 (2015)
38. A. Raza, L. Feng, X. Xu, J. Tang, International journal of biological macromolecules 94 (Part A), 335–344 (2017)
39. Z. Ying, X. Han, J. Li, Food Chem. **127**(3), 1273–1279 (2011)
40. J. Maran, B. Priya, Int. J. Biol. Macromol. **70**, 530–536 (2014)
41. R. Contamine, A. Wilhelm, J. Berlan, H. Delmas, Ultrason. Sonochem. **2**(1), S43–S47 (1995)
42. J. Zhang, C. Wen, W. Qin, P. Qin, H. Zhang, Y. Duan, Int J Biol Macromol 118 (Pt B), 2269–2277 (2018)
43. W. Sheng, Z. Ling, L. Qing et al., Food Hydrocoll. **91**, 34–39 (2019)
44. Y. Yi, H. Hua, X. Sun, Y. Guan, C. Chen, Spectrochim. Acta Part A Mol. Biomol. Spectrosc. **240**(15), 118623 (2020)
45. X. Zou, J. Zhao, M. Povey, M. Holmes, H. Mao, Anal. Chim. Acta **667**(1), 14–32 (2010)

Figures

Figure 1

Ultraviolet, molecular weight, monosaccharide composition, FT-IR spectrometric of *S.sagittifolia* L. polysaccharides (Sap). (A) The UV scanning wavelength was in the range of 200-400 nm; (B) High performance size exclusion chromatograph

profile of Sap; (C) Gas chromatographic profile of Sap; (D) The FT-IR spectra of sample was in the range of 4000-500 cm^{-1}.

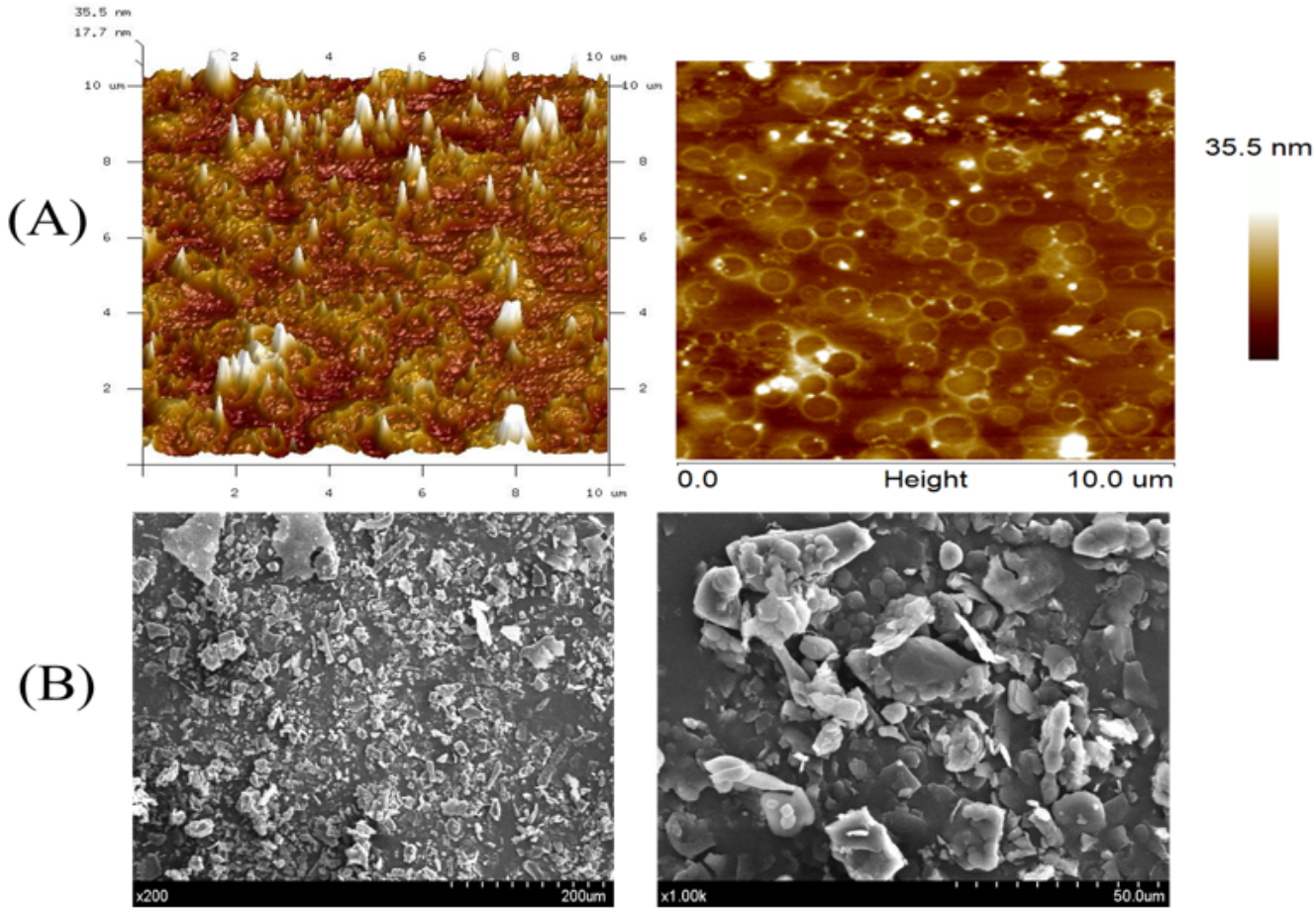

Figure 2

Morphological properties of Sap. (A) AFM images, (B) Scanning electron micrographs (200×, 1000×).

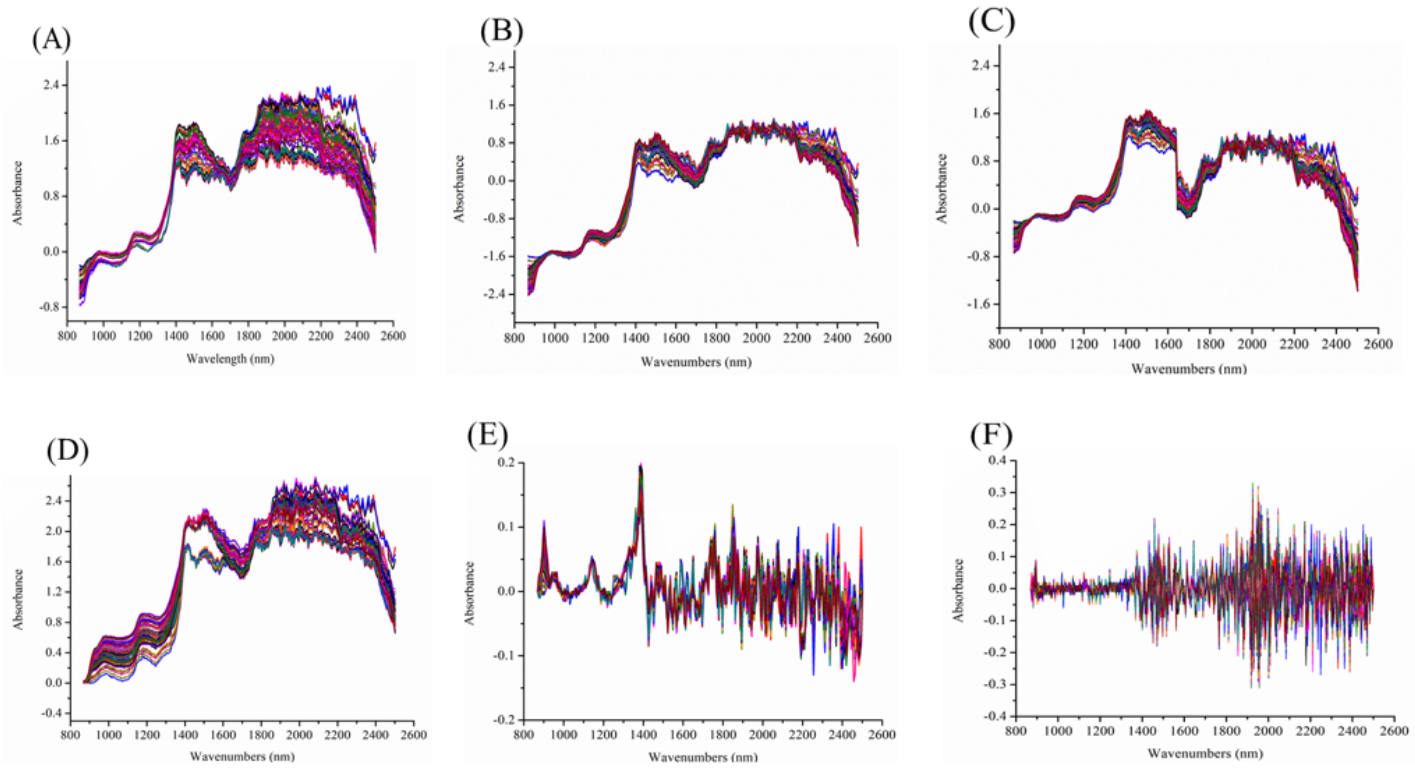

Figure 3

The NIR spectral preprocessing Sap. (A) Raw spectra; (B) SNV spectra; (C) MSC spectra; (D) Baseline spectra; (E) Derivative I spectra; (F) Derivative II spectra.

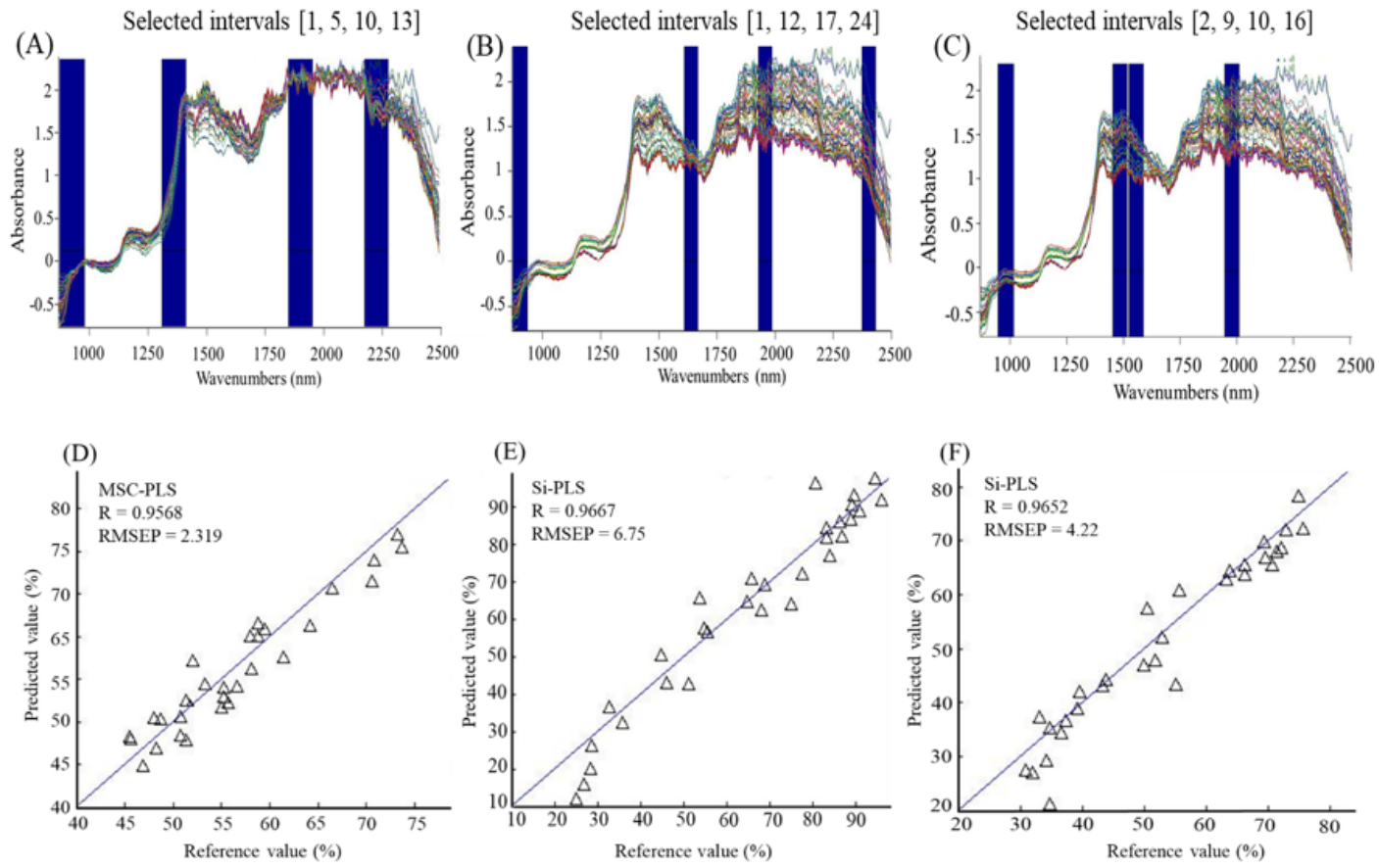

Figure 4

The optimal spectral intervals of Si-PLS and the scatter plot of the optimal model in the prediction sets. (A) the optimal spectral intervals of DPPH; (B) the optimal spectral intervals of ABTS; (C) the optimal spectral intervals of hydroxyl radical; (D) MSC-PLS model of DPPH; (E) Si-PLS model of ABTS; (F) Si-PLS model of hydroxyl radical.

Supplementary Files

This is a list of supplementary files associated with this preprint. Click to download.

- Supplementarymaterial.docx